High resolution absolute temperature mapping of laser crystals in diode-end-pumped configuration

Julien Didierjean[1], Sébastien Forget[1], Sebastien Chenais, Frédéric Druon[1], François Balembois[1], Patrick Georges[1], Konrad Altmann[2], Christoph Pflaum[3]

[1]Laboratoire Charles Fabry de l'Institut d'Optique, UMR 8501, Centre Universitaire, Bât. 503, 91403 Orsay Cedex, France.
[2]LAS-CAD GmbH, Brunhildenstr, 9, 80639 Munich, Germany, Phone +49 89 173607, Fax +49 89 172594, Dr.Altmann@las-cad.com
[3]Universtät Erlangen, Lehrstuhl für informatik X, Cauerstr. 6, 91508 Erlangen, Germany, pflaum@informatik.uni-erlangen.de

ABSTRACT:

We report on direct, absolute and spatially resolved temperature measurements in various diode-end-pumped laser crystals, using an infrared camera. Our measurement method requires careful calibrations of the camera, to take into account the emissivity of the crystals. We tested the repeatability of the calibration process, and the linearity of calibrations curves was verified to up to 100°C. We also compared our experimental results with finite elements analysis simulations done with LASCAD. We used our setup to compare different types of thermal contacts and to measure the corresponding heat transfer coefficients using an Yb:YAG crystal. Finally we compared the thermal behaviour of Nd:YVO$_4$ and Nd:GdVO$_4$ crystals under the same pumping conditions.

1. INTRODUCTION:

End pumped bulk laser crystals are good candidates to high power and high beam quality lasers, but they are mainly limited by thermal effects. Thermal lensing, depolarisation losses and induced stress can lead to power losses, beam quality degradation or even fracture of the crystal [1]. A better understanding of thermal issues is therefore needed to proceed to higher laser power.

The most widespread way to investigate thermal effects in laser crystals is to use thermo-optical methods, that is thermal lens measurements or depolarization measurements. However, these methods only yield quantities that are proportional to thermal gradients inside the probed area, and they depend on the values of more or less known thermo-optical coefficients. Similarly, temperature distributions obtained by finite element analysis depend on material parameters which are not always well known or cannot be directly measured for instance the heat efficiency.

Therefore, a direct method leading to absolute temperature mapping with high resolution is highly desirable [2]. In this paper we present this kind of analysis for end-pumped configurations, based on an infrared camera sensitive in the 8-12 μm range. Our method enables us to measure the temperature map of the end-pumped face of the crystal. In the first section, the experimental setup will be described. In a second section, the calibration method will be detailed, and in the third part some experimental results will be compared with simulations, as a validation test. After this validation, our method will be used in the fourth and fith part to measure heat transfer coefficients with an Yb:YAG crystal and to compare Nd:YVO$_4$,and Nd:GdVO$_4$ thermal performances.

2. EXPERIMENTAL SETUP:

The experimental setup is shown in figure 1. The thermal imaging was obtained thanks to a dichroic Zinc selenide plate, High Reflectivity (HR) coated for 800-1080 nm on one face (at 45° angle of incidence), and also coated for High Transmission (HT) in the 8-12 μm spectral range on both faces. An aberration-free germanium objective (focal length 50 mm, N.A. 0.7) was appended close to the ZnSe plate to create the intermediate thermal image. The camera was an AGEMA 570 (*Flir Systems Inc*.) consisting of 240x320

microbolometers working at room temperature. The measured noise equivalent temperature difference (NETD) of the camera is 0.2 °C. The numerical aperture of the whole imaging system in the object medium being around 1, a theoretical spatial resolution of 10 μm could be achieved; however, the resolution is here limited to 60 μm by the size of the pixels. One has to notice that measures are not disrupted by the thermal emission of the bulk because laser crystals are not transparent in the 8-12 μm range.
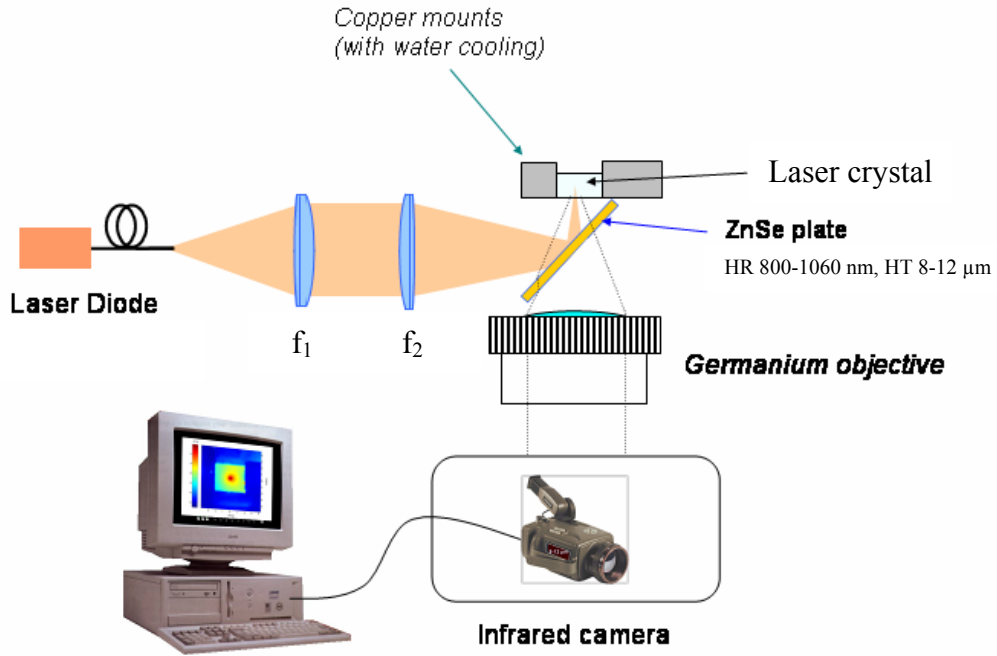

Fig. 1: Experimental setup

We used two fiber-coupled laser diodes depending on the crystal tested:
For experiments with Yd-doped crystals, the pump source was a high power fiber-coupled diode array (HLU15F200-980 from LIMO GmbH) emitting 13.5 W at 968 nm. The fiber had a core diameter of 200 μm and a numerical aperture of 0.22. The output face was imaged onto the crystal to a 270-μm spot in diameter via two doublets (f_1 = 60 mm, f_2 = 80 mm).

For experiments with Nd-doped crystals, the pump source was a high power fiber-coupled diode array (Thales laser diode) emitting 15 W at 808 nm. The fiber had a core diameter of 800 μm and a numerical aperture of 0.22. The output face was imaged onto the crystal to a 1300 or 800-μm spot in diameter via two doublets (f1 = 60 mm, f2 = 100 or 60 mm, respectively).

3. CALIBRATIONS

The IR camera is sensitive to the spectric luminance emitted by the laser crystal and to the background infrared noise integrated on the spectral band of sensitivity of the microbolometers. The signal incident on the camera is:

$$\left[\frac{dL}{d\lambda}\right]_{Crystal}^{Tcrystal} = \varepsilon.\left[\frac{dL}{d\lambda}\right]_{Black\_Body}^{Tcrystal} + \left[\frac{dL}{d\lambda}\right]_{other\_sources}^{indep.\_of\_Tcrystal} \qquad (1)$$

Where :

$\left[\frac{dL}{d\lambda}\right]_{Crystal}^{Tcrystal}$ is the total spectric luminance emitted by the crystal at the temperature $T_{crystal}$.

2

ε is the emissivity of the crystal.

$\left[\dfrac{dL}{d\lambda}\right]^{Tcrystal}_{Black\_Body}$ is the spectric luminance emitted by the crystal at the temperature $T_{crystal}$.

$\left[\dfrac{dL}{d\lambda}\right]^{indep.\_of\_Tcrystal}_{other\_sources}$ is the spectric luminance emitted by other sources of the observed area, independently of the crystal temperature

But the camera software considers the crystal as a black body. Calculating the temperature on the basis of the incident infrared power, the detector gives a temperature $T_{measured}$, smaller than $T_{crystal}$, verifying :

$$\left[\dfrac{dL}{d\lambda}\right]^{Tcrystal}_{Crystal} = \left[\dfrac{dL}{d\lambda}\right]^{Tmeasured}_{Black\_body}$$

Using the Stefan law, one can write:

$$K_3 . T^4_{measured} = \varepsilon . K_3 . T^4_{crystal} + L_{other\_sources} \qquad (2)$$

Where $K_3 = 1.804 \cdot 10^{-8}$ W.m^{-2}.sr^{-1}.K^{-4} is the Stefan constant. Finally we can express $T_{crystal}$:

$$T_{crystal} = \left(\dfrac{1}{\varepsilon} . T^4_{measured} - L_{other\_sources}\right)^{1/4} \qquad (3)$$

with $\varepsilon = 0.7$ and $L_{other\_sources} = 2.5 \ 10^9$ W.m^{-2}.sr^{-1}, one can plot the curve of figure 2:
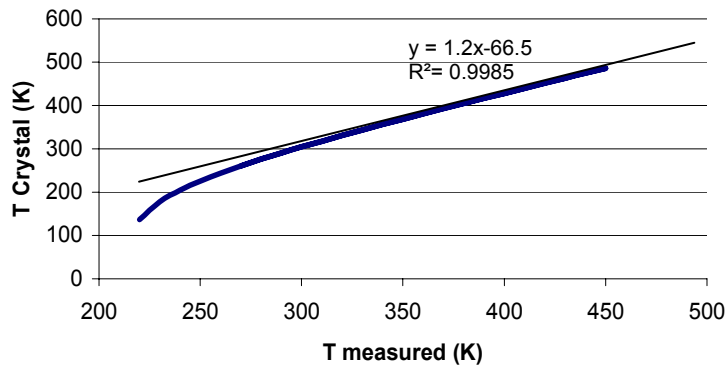

Fig 2: Theoretical relation between real temperature in the crystal and measured temperature

For temperature higher than 300K, the relation between the real and measured temperature is approximately linear: $T_{réelle} = a . T_{mesurée} + b$. So we only need to know **a** and **b** to deduce the real map of temperature from the map measured by the detector. Those coefficients are different for every crystal, so we need to make calibrations for every sample we used. To find the value of **a** and **b**, we used the setup shown in figure 3. The crystal and its mount are uniformly heated to a given temperature by a peltier device, and we record the corresponding temperature measured by the camera. The ZnSe plate is not necessary as there is no pump light incident on the crystal, but we let it in place so the experimental conditions are the same for the calibration and the measurement.
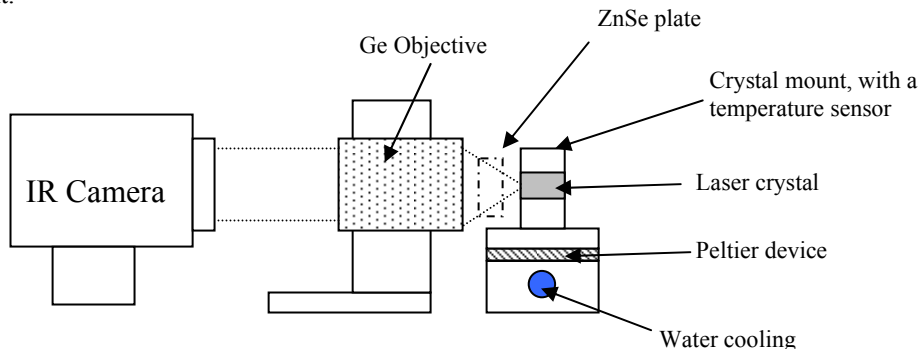

3

Fig 3: Calibration setup

The calibration results are shown in figure 4 for a Nd:YAG crystal, 1% doped, with high transmission coating for λ = 808 nm and λ = 1064 nm. In agreement with theoretical calculations, we found that the relation between the real temperature of the crystal and the temperature measured by the camera is linear. A numerical program has been developed to deduce automatically the real temperature maps from the measured maps using the parameters of the calibration curves.
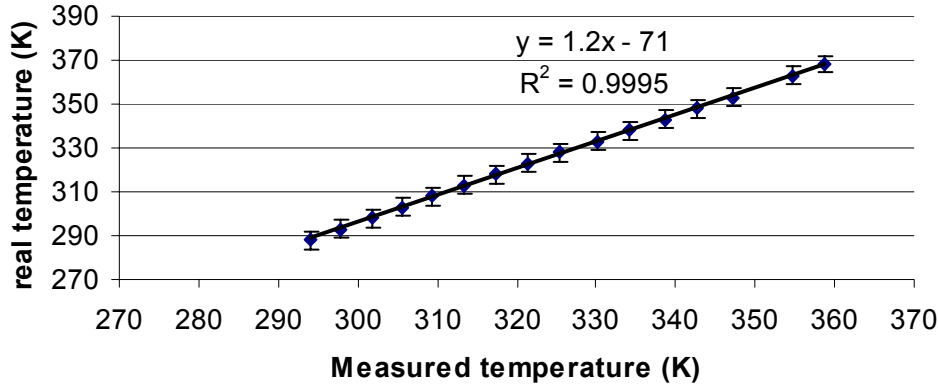

Fig 4: Calibration curve of a Nd:YAG 1at.% doped crystal

The linearity of the calibration curves has been verified to temperature as high as 360K, and the incertitude due to the calibration process is less than 4°C. The calibrations curves were measured for other crystals with similar results.

4. LASCAD SIMULATIONS

Finite element analysis codes are a common way to investigate the thermal behaviour of laser systems. However, the results of those simulations have not been be checked so far by direct measurements. Our temperature mapping method enables us to do this verification, so we compared our experimental results with the FEA simulations of the LASCAD software [3] for a Nd:YAG 1.0at.% and a Nd:YVO$_4$ 1.0at.% crystals.

Finite Element Analysis

To solve the differential equations for thermal and structural analysis (thermal deformation), we applied a finite element discretization on semi-unstructured grids [4][5] that have properties which are very useful in the application of laser simulation:

- Semi-unstructured grids calculate temperature distribution and deformation on a structured grid inside of the crystal which is very well suited for the analysis and interpolation of the data in a subsequent optical analysis of the cavity. This structured grid is connected to the surface of the crystal by small irregular elements.
- Semi-unstructured grids allow using fast computational codes. Different from irregular meshing computational time increases linearly with the number of grid points.
- Semi-unstructured grids can be stretched in x-, y-, and z-direction.
- High accuracy can be achieved by the use of small mesh size.
- The super-convergence of the gradient inside of the domain leads to an accurate approximation of the stress.

Our code is implemented in the laser simulation program LASCAD. In the present case, heat load distribution has been approximated by the use of supergaussian functions in combination with an absorption coefficient. Boundary conditions have been defined by keeping the lateral surfaces of the crystal on constant temperature.

Comparison between measurements and simulation

Both crystals were end-pumped by the laser diode at λ = 808 nm described in the section 2. They were placed in a 4-side copper mount with a water cooling system. The pump beam profile was gaussian.

4

The Nd:YAG 1.0at.% crystal was 4 mm long, with a square cross section of 2 mm. The incident pump beam was focused inside the crystal, at 0.5 mm of the entrance face. The diameter of the pump spot was 1300 μm, with a divergence of 125 mrad. The incident power was 8.5 W. The experimental and simulated temperature profiles are plotted in figure 5.
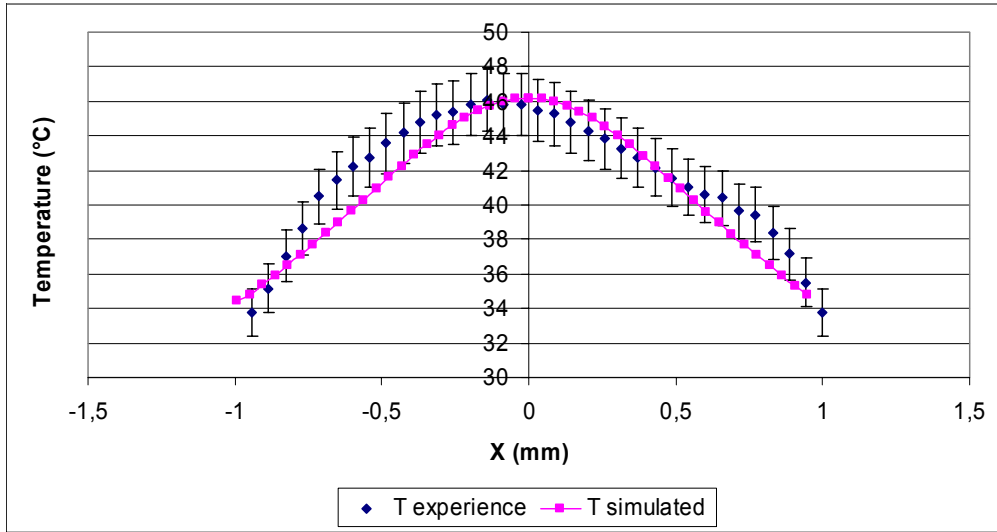

Fig 5: Measured and computed distribution of temperature T for Nd:YAG 1.0at.%
at the entrance plane of the pump beam.

To fit the computed curves to the measured ones, a global heat efficiency factor has been used describing the fraction of pump power converted into heat. We obtained good agreement for a heat efficiency of 0.27 which is close to the commonly reported factor 0.33, see for instance [6]. With this parameter, the agreement between simulation and experiment is quite good, as the general shape and the temperature values are nearly the same. The non-symmetric shape of the experimental curve is due to a slight dissymmetry of the pumping configuration.

The Nd:YVO$_4$ 1.0at.% crystal was 5 mm long, with a square cross section of 3 mm. The pump beam was focused 0.2 mm after the entrance face of the crystal. The diameter of the pump spot was 800 μm, with a divergence of 125 mrad, and the incident power was 7.5W. The experimental and computed temperature profiles are plotted in figure 6.

Fig 6: Measured and computed distribution of temperature T for Nd:YVO$_4$ 1.0 at. %
at the entrance plane of the pump beam.

We used a heat efficiency factor 0.32 to fit the curves, which is a bit higher than the factor 0.24 reported by Chen and Kuo [7] for lasing conditions. This deviation however may be explained by the fact that laser power extraction reduces the fraction of pump power converted into heat which is not the case in our experiments. The

shape of those curves is quite different from those plotted for the Nd:YAG crystal because the pump spot is smaller and because the thermal conductivity of Nd:YVO$_4$ crystals is lower than the one of Nd:YAG crystals.

As a conclusion, the simulations were fitted with the experiments using reliable values for the heat efficiencies, with tow different crystals and in different pumping conditions. The agreement observed validated our temperature mapping method.

5. HEAT TRANSFER MEASUREMENTS WITH YB:YAG CRYSTAL

One of the most important features of a solid-state laser system is the quality of the crystal cooling. To ensure a good heat removal, it's necessary that the heat transfer between the crystal and its mount is as good as possible. Measures of the heat transfer coefficient are usually difficult, but our thermal mapping method enables us to make it in a simple manner. We used it to compare different types of thermal contacts with a well-known crystal, the Yb:YAG. The crystal used was 2 mm long, 4*4 mm² square cross section, 8at.%. It was placed in a 4 side copper mount with different type of thermal contact (Bare contact, graphite layer, indium foil, and heat sink grease). The results presented here have already been published in [2]. The experimental setup is described in Section 1.

Figure 7 shows the temperature map obtained when the crystal is clamped by its four edge faces by bare contact with copper without thermal joint (left part) and with heat sink grease (right part). In the first case, a clear gap is noticeable between the temperatures of the mount and at the edge of the crystal. The temperature distribution is parabolic inside the pumped region and then experiences a logarithmic decay until the edge of the crystal, in good agreement with the theory in the case of fiber-coupled diode pumping. The temperature difference at the centre of the crystal between the two types of thermal contact shows clearly the importance of the interface.
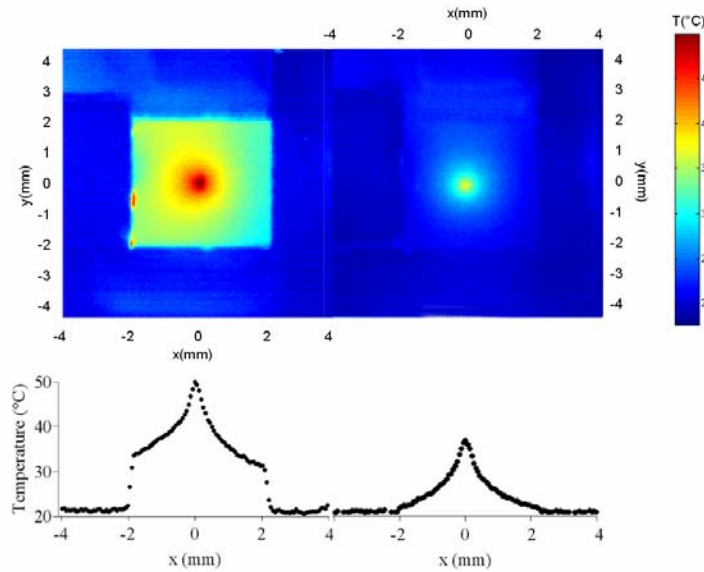

Fig 7: temperature mapping of the crystal (front view) and lateral cut at y=0 for two different types of thermal contact (direct copper-crystal contact on the left, with grease on the right).

We consequently studied more in details the heat contact. By analogy with convective transfer, the quality of the contact can be accounted by a heat transfer coefficient H (in W.cm^{-2}.K^{-1}), defined so that the heat flux through the surface is[3]:

$$ - K_c \left\| \vec{\nabla} T \right\|_e = H \left(T_e - T_m \right) \qquad (4) $$

where K_c is the thermal conductivity of the crystal (W.cm^{-1}.K^{-1}), T_e the temperature at the edge of the crystal and T_m the heat sink temperature. The thermal gradient in (4) is considered normal to the surface. An ideal contact ($T_e = T_m$) corresponds to an infinite value of H.

By performing a linear fit of the temperature versus position on the points that are closer to the crystal edge, the heat flux can be determined: by applying relation (4), one can then infer the value of H, which is here equal to 0.25 $W.cm^{-2}.K^{-1}$ in the case of bare contact. We estimate that the uncertainty on H is about 15%. The order of magnitude obtained is consistent with the values evoked by Carslaw[3] and Koechner[4]. A hot spot can be noticed in figure 7, which betrays the poor contact between the polished face of the crystal and the copper surface.

We have then tested four different types of contacts between the crystal and the copper: bare contact, graphite layer, indium foil and heat sink grease. The results are summarized in table 1.

Contact	H ($W.cm^{-2}.K^{-1}$)	T_{max} (°C)	T_e (°C)	T_e-T_m (°C)
Bare	0.25	49.8	33.5	10.7
Graphite layer	0.28	46.5	30.5	8.7
Indium foil	0.9	40.0	25.1	4.9
Heat sink grease	2.0	37.0	21.6	1.5

Table 1: Experimental results. T_{max} is the temperature at the centre of the pumped region; T_e is the temperature at the edge of the crystal (averaged on the 4 sides if not symmetrical), and T_m is the copper mount temperature near the crystal.

Those results show there is little improvement between bare contact and graphite layer. The indium foil gives better results, reducing significantly the maximum temperature and the gradient inside the crystal. But the best results were given by the use of heat sink grease. The grease has an excellent thermal conductivity and it is fluid enough to fill the gaps between the crystal and its mount. Obviously those results are not specific to Yb:YAG laser systems, and can be applied to other crystals as well.

6. THERMAL BEHAVIORS OF Nd:YVO$_4$ AND Nd:GdVO$_4$

Our absolute thermal mapping measurements can also be used to compare the thermal behavior of different laser crystals. We chose to study two Nd-doped materials, the YVO_4 and the $GdVO_4$ crystals.

Nd:GdVO$_4$ is a recent but widely used crystal. It has similar optical proprieties than the Nd:YVO$_4$, but his thermal conductivity K_c is better. The exact value of this conductivity is not known, as many publications announce quite different results. In the literature, one can find conductivity values ranging from 8 W/mK to 12 W/mK for the Nd:GdVO$_4$, whereas for the Nd:YVO$_4$ crystal K_c vary around 5 W/mK [8][9][10]. According to calculations, a better thermal conductivity would decrease the thermal gradients inside the crystal, so the maximal temperature observed on the end-pumped face should decrease. To verify those statements, we realized measurements with a set of the two crystals coming from the same manufacturer, with same doping concentration.

We used the following samples for our experiments:

- 3 Nd:YVO$_4$ crystals, doped at.1%, square cross section 3*3 mm, 5 mm long
- 2 Nd:GdVO$_4$ crystals, doped at. 1%, square cross section 3*3 mm, 5mm long

Our experimental setup enables us to measure the temperature map of the end-pumped face of the crystals. To compare fairly the two crystals, we need to be sure that they absorb the same pump power on this face:

$$\frac{dP}{dz}_{(z=0)YVO_4} = \frac{dP}{dz}_{(z=0)GdVO_4} \qquad (5)$$

The absorption of the neodymium is an exponential law, but the absorption coefficient α depends on the polarization. So we separated the π and σ polarization of the pump light with a polarizer placed in the collimated pump beam. The (5) condition then becomes as following:

$$\begin{cases} \alpha_{Nd:YVO_4\pi}.P_{(z=0)} = \alpha_{Nd:GdVO_4\pi}.P_{(z=0)} \\ \alpha_{Nd:YVO_4\sigma}.P_{(z=0)} = \alpha_{Nd:GdVO_4\sigma}.P_{(z=0)} \end{cases}$$

Those conditions can be realized by adjusting the absorption coefficient by detuning the pump wavelength from the peak of absorption. The wavelength emitted by the pump laser diode is controlled by the temperature regulation of the diode junction.

Experimental conditions:

The polarized incident pump power $P_{(z=0)}$ was 6 W. Crystals were placed in a four edge copper mount, water cooled, and the thermal contact between the crystals and the mount was assured by a 0.5 mm indium foil. We verified that our temperature measurements were not dependent with the experimental conditions by removing crystals, changing the indium foils and replacing them in the mount. The repetability was found to be very good.

The focalization lens of the experimental setup (f_2 in figure 1) was set to 60 mm, so the diameter of the pump spot in the crystal was 800μm.
For our experiments we chose:

$$\frac{dP}{dz}_{(z=0)_\sigma} = 5.0 \text{ W/mm}$$

$$\frac{dP}{dz}_{(z=0)_\pi} = 4.3 \text{ W/mm}$$

Experimental Results:

The maximum temperature and the temperature gradient (between the center of the pump spot and the edge of the crystal) of the end-pumped face are given for every sample of the tow crystals in table 2 and 3. The incertitude on the determination of the dP/dz factor is about 5%.

On the σ polarization :

crystal	dP/dz (W/mm)	Tmax (°C)	gradient (°C)
YVO4 1	4.3	126	60.9
YVO4 2	4.4	120	55.4
YVO4 3	4.3	117	56.1
		121 +/- 5°C	**57.5 +/- 3.5 °C**

crystal	dP/dz (W/mm)	Tmax (°C)	gradient (°C)
GdVO4 1	4.3	117	58.2
GdVO4 2	4.4	123	55.2
		120 +/- 3°C	**56.7 +/- 2°C**

Table 2: maximum and gradient of temperature on the end-pumped face of the crystals for a σ polarized pump beam.

On the π polarization:

crystal	dP/dz (W/mm)	Tmax (°C)	gradient (°C)
YVO4 1	5.0	153	93.5
YVO4 2	5.1	169	95.3
YVO4 3	5.1	147	88.5
		156 +/- 13°C	**92.4 +/- 4°C**

crystal	dP/dz (W/mm)	Tmax (°C)	gradient (°C)
GdVO4 1	5.0	157	94.1
GdVO4 2	5.1	166	93.4
		161.5 +/-5°C	**93.7 +/- 1°C**

Table 3: maximum and gradient of temperature on the end-pumped face of the crystals for a π polarized pump beam.

Results are very similar for the two crystals. No temperature decrease was observed with Nd:GdVO$_4$ crystal. This result is quite surprising, and more experiments are necessary to verify and understand it. There is two main possible explanations:

- The K$_c$ of our samples are similar for YVO$_4$ and GdVO$_4$ crystals. As the conductivity values are not very well known or controlled for those crystals, it is a possible solution.
- There are more heating parasite effects in our GdVO4 crystals, rising the temperature despite of the better thermal conductivity. This is possible as the GdVO4 is a quite recent crystal witch is difficult to grow.

7. CONCLUSIONS

In this paper we demonstrated the realization of a thermal mapping method of end-pumped laser crystals. We checked the validity of our calibration method, and the agreement between experiment and theoretical temperature maps at the crystal input surface were found to be very good in two different configurations. We have used our experimental setup to calculate by a simple method the heat transfer coefficient between a crystal and its mount, for different type of thermal contacts, and shown that the thermal grease represent the best thermal contact we have tested. Finally we have done the first direct thermal behavior comparison between Nd:YVO4 and Nd:GdVO4 crystals.

The next step of our work will be to measure temperature map under lasing conditions. It would enable us to see directly the effect of stimulated emission on the thermal load of various laser crystals. We also foresee to complete our temperature mappings with thermal lens measurements.

REFERENCES:

1. W.A.Clarkson, "Thermal effects and their mitigation in end-pumped solid-state lasers", *J.Phys.D: Appl. Phys.,* **34**, 2381 (2001).

2. S. Chenais, S. Forget, F. Druon, F. Balembois, P. Georges, "Direct and absolute temperature mapping and heat transfer measurements in diode-end-pumped Yb:YAG", *Appl. Phys. B.,* **79**, 221 (2004).

3. LASCAD^{TM}, http://www.las-cad.com.

4. Ch. Pflaum, "Semi-unstructured grids", *computing*, **67**, 141 (2001).

5. K. Altmann, Ch. Pflaum, D. Seider, "Semi-unstructured grids in the laser simulation program LASCAD", *Proceeding of GAMM 2002* (2002).

6. T.Y. Fan, "Heat generation in Nd:YAG and Yb:YAG ", *IEEE J. of Q. El.,* **29**, 1457 (1993).

7. Y.F. Chen, H.J. Kuo, "Determination of thermal loading of diode pumped Nd:YVO4 by use of thermally induced output depolarization", *Opt. Lett.*, **23**, 846 (1998).

8. L.J. Qin, X.L. Meng, H.Y. Shen, L. Zhu, B.C. Xu, L.X. Huang, H.R. Xia, P. Zhao, G. Zheng, *Cryst. Res. Technol.*, **38**, 793 (2003).

9. J. Petit, B. Viana, P. Goldner, D. Vivien, P. Louisseau, B. Fernand, "Laser oscillation with low quantum defect in Yb:GdVO4, a crystal with high thermal conductivity", *Opt. Lett.,* **29**, 833 (2004).

10. C. Kränkel, D. Fagundes-Peters, S.T. Fredrich, J. Johannsen, M. Mond, G. Huber, M. Bernhagen, R. Uecker, "Continuous wave laser operation of Yb^{3+}:YVO4", *Appl. Phys. B*, **79**, 543 (2004).